(2)

03/05/93

Atomic-Scale Friction Measurements Using Friction Force Microscopy Part II-Application to Magnetic Media

Bharat Bhushan (Fellow ASME) and Ju-Ai Ruan
Computer Microtribology and Contamination Laboratory
Department of Mechanical Engineering
The Ohio State University
Columbus, Ohio 43210-1107

Abstract

Atomic Force/Friction Force Microscopes (AFM/FFM) were used to study tribological properties of metal-particle tapes with two roughnesses, Co-γFe_2O_3 tapes (unwiped and wiped), and unlubricated and lubricated thin-film magnetic rigid disks (as-polished and standard textured). Nanoindentation studies showed that the hardness of the tapes through the magnetic coating is not uniform. These results are consistent with the fact that the tape surface is a composite and is not homogeneous. Nanoscratch experiments performed on magnetic tapes using silicon nitride tips revealed that deformation and displacement of tape surface material occurred after one pass under light loads (~ 100 nN). A comparison between friction force profiles and the corresponding surface roughness profiles of all samples tested shows a poor correlation between localized values of friction and surface roughness. Detailed studies of friction and surface profiles demonstrate an excellent correlation between localized variation of the slope of the surface roughness along the sliding direction and the localized variarion of friction. Atomic-scale friction in magnetic media and natural diamond appears to be due to adhesive and ratchet (roughness) mechanisms. Directionality in the local variation of atomic-scale friction data was observed as the samples were scanned in either direction, resulting from the scanning direction and the anisotropy in the surface topography. Atomic-scale coefficient of friction is generally found to be smaller than the macro coefficient of friction as there may be less ploughing contribution in atomic-scale measurements.

1. Introduction

Magnetic tapes and disks are widely used recording media in the information storage (audio, video, and data processing) industry. The recording (writing) and retrieving (reading) of the information to and from these media require the relative motion between a read/write head and a medium (Bhushan, 1990). Formation of air bearing minimizes the head-medium contact. However, physical contact between the head amd medium occurs during starts and stops. The need for ever increasing recording densities requires that the head and medium surfaces be as smooth as possible and the flying height be near zero (contact recording). In order to miniaturize magnetic storage devices and to minimize friction and wear at the head-medium interface, the size of head components is reduced. Microfabrication techniques allow the mass production of small heads on a sub-mm scale (Bhushan et al., 1992). These heads would be very light (on the order of a microgram) and would operate under very light loads (on the order of few milligrams). As a result, friction and wear of lightly loaded microcomponents are highly dependent on the surface interactions (few atomic layers). As these microfabricated heads become reality, the study of tribology on a nanoscale (generally referred to as "microtribology") becomes a necessity. Atomic force/friction force microscopes (AFM / FFM) have been developed for microtribological studies (Mate et al., 1987; Kaneko, 1988; Meyer and Amer, 1988, 1990; Kaneko et al., 1991; Ruan and Bhushan, 1993).

In the construction of particulate magnetic tapes and flexible disks, submicron magnetic particles are dispersed in a polymeric matrix and coated onto a polymeric substrate. About 1 to 7% by weight fatty acid ester is added to the coating for lubrication. In thin-film rigid disks, a continuous film of magnetic material is deposited onto aluminum or glass substrates by vacuum deposition techniques. For wear and corrosion protection, the magnetic film is coated with 20 to 30-nm thick diamondlike carbon (DLC) coating and 0.5 to 2-nm thick perfluoropolyether (PFPE) lubricant coating. To reduce stiction and friction, the disk substrate is textured (Bhushan, 1990).

For an optimized roughness distribution for the tape and disk surfaces, it is important to understand the relationship between localized variations in the surface roughness and friction. The lubricant film in magnetic disks does not have uniform distribution (Mate et al., 1989; Bhushan and Blackman, 1991). As a result, the friction behavior could vary locally. A number of papers on AFM/FFM studies of magnetic thin-film disks have appeared in the literature (Blackman et al., 1990a, 1990b; Miyamoto et al., 1990; Bhushan and Blackman 1991; Kaneko et al., 1991; Andoh et al., 1992; Hamada and Kaneko 1992; Mate, 1992). Kaneko et al. (1991) were unable to establish any relationship between local variations in friction and surface roughness. AFM imaging data of magnetic tapes was presented by Oden et al. (1992). No papers exist on FFM data of magnetic tapes.

In this paper, we present nanohardness, nanoscratch and atomic-scale friction measurements on various tapes and disks. We present an analysis to establish correlation between localized variation in friction and surface roughness data. A polished natural diamond was also measured for reference, for the purpose of eliminating any effect which may be result from changes in chemical composition of the sample surface. The atomic-scale friction data have been compared with macroscopic data.

2. Experimental

2.1 Description of AFM / FFM and Measurement Techniques

We used an AFM/FFM to conduct hardness/scratch, and friction measurements. Friction measurement technique has been described in a companion paper by Ruan and Bhushan (1993). The AFM/FFM used here can provide simultaneous measurements of friction force and surface roughness. The sample is mounted on a piezoelectric tube (PZT) scanner which can precisely scan the sample in the horizontal (x-y) plane and can move the sample in the vertical (z) direction. A sharp tip at the free end of a Si_3N_4 beam is brought in contact with the sample. A laser beam from a laser diode is focused onto the back of the cantilever near its free end. The cantilever is tilted

downward at about 10^0 with respect to the horizontal plane. The beam is reflected from the cantilever and is directed through a mirror onto a split photodetector with four quadrants. Two quadrants (top and bottom - T and B) of the detector are used during the measurement of the topography of sample surface. As the sample is scanned under the tip, topographic features of the sample cause the tip to deflect in vertical direction. This tip deflection will change the direction of the reflected laser beam, changing the intensity difference between the top and bottom photodetector (AFM signal). A feedback circuit is used to modulate the voltage applied to the PZT scanner to adjust the height of the PZT, so that the cantilever vertical deflection or the normal force (given by the intensity difference between the top and bottom detector) will remain almost constant during scanning. Thus the PZT height variation is a direct measure of surface roughness of the sample.

In nanoindentation studies, sample was loaded in contact with the tip. During loading, tip deflection (normal force) was measured as a function of z position of the sample. For a rigid sample, the tip deflection and the sample traveling distance (when the tip and sample come into contact) equal to each other. Any decrease in the tip deflection as compared to z position of the sample represented indentation. In nanoscratch studies, sample was scanned twice at each of the two normal loads: 10 and 100 nN. Any changes in the topography were believed to occur as a result of local deformation of the sample surface.

A preferred method of measuring friction force is described by Ruan and Bhushan (1993). In this method, the other two (left and right) quadrants of the photodetector (arranged horizontally) are used for the measurement of friction force being applied at the tip. The sample is scanned back and forth in a direction perpendicular to the longitudinal axis of the cantilever beam. Friction force between the sample and the tip will produce a twisting of the cantilever. The laser beam will be reflected out of the plane defined by the incident beam and the beam reflected vertically from an untwisted cantilever. This produces an intensity difference of the laser beam received between the

left and right quadrants of the photodetector. The intensity difference between the left and right detectors (FFM signal) is directly related to the degree of twisting, hence to the magnitude of friction force. One problem associated with this method is that any misalignment between the laser beam and the photodetector axis would introduce error in the measurement. By adding the average of the two FFM signals obtained by scanning the sample in two opposite directions and dividing by two, and then substracting this component from either profiles, the misalignment effect can be eliminated. By following normal force and friction force calibration procedures developed by Ruan and Bhushan (1993), voltages corresponding to normal and friction forces can be converted to force units. By making measurements at various normal loads, average value of coefficient of friction is obtained which then can be used to convert the friction profile to the coefficient of friction profile. Thus, any directionality and local variation of friction can be easily measured. Surface topography data can be measured simultaneously with the friction data and local relationship between the two profiles can be established. During AFM /FFM measurements, typical scanning speed was 500 nm/s and stepping speed in the perpendicular direction was 4 nm/s for a 1μm x 1μm area. Speed was increased by a factor of ten for a 10 μm x 10 μm scan, and decreased correspondingly for smaller area scans. Average values of coefficient of friction were measured over both 1 μm x 1 μm and 10 μm x 100 μm scan areas. Local variation of friction were measured over smaller areas (0.4 or 0.5 μm) for clarity.

For comparisons, macroscopic friction measurements were also made using various apparatuses. For magnetic tapes, two different reciprocating testers were used. In one of the apparatus, a tape was wrapped over a Ni-Zn ferrite rod and slid in a reciprocating motion with a 0.2 N load attached on one end and a load cell attached on the other end. The tape was reciprocated at a speed of about 60 mm/s (Bhushan, 1990). In the other tester, a silicon nitride ball (5-mm diameter with 3-nm rms roughness) was reciprocated against a tape surface mounted on a reciprocating table under the following conditions: reciprocating amplitude=0.8 mm, frequency=1 Hz, and normal load=0.2 N. For macrofriction measurements of magnetic disks, a Al_2O_3-TiC

slider was slid against a disk at a normal load of 0.1 N and sliding speed of 0.4 m/s (Bhushan and Venkatesan, 1993).

2.2 Test Samples

For this study, four tapes and four disks were selected. Two 12.7-mm wide and 13.2-μm thick (base thickness of 9.8 μm, magnetic coating of 2.9 μm, and back coating of 0.5 μm) metal-particle (MP) tapes with rms roughness of about 5 nm (calendered tape) and of about 10 nm (uncalendered tape) were selected to study the effect of roughness. Two 12.7-mm wide and 17-μm thick (back coated) Co-γ Fe_2O_3 tapes were selected before and after wipe to study the effect of wipe material. [Webs are wiped before slitting and slit webs (tapes) are further wiped to remove any contaminants.] Two thin-film rigid disks with a polished substrate and other two with a standard textured substrate, with and without a bonded perfluoropolyether were selected. These disks were 95-mm in diameter made of Al-Mg alloy substrate (1.3 mm thick) with a 10 to 20-μm thick electroless plated Ni-P coating, 75-nm thick ($Co_{79}Pt_{14}Ni_7$) magnetic coating, 20 to 30-nm thick diamondlike carbon (~1500 kg/mm^2) coating, and with or without top layer of lubricant coating.

3. Results and Discussion

3.1 Nanoindentation and Nanoscratch

We first present the nanoindentation results of two metal-particle tapes shown in Fig. 1. In this figure, the vertical axis represents the cantilever deflection and the horizontal axis represents the vertical (z) position of the sample. The "extending" and "retracting" curves correspond to the sample being moved towards or away from the cantilever tip respectively. In this experiment, as the sample surface approaches the AFM tip within a few nm (point A), an attractive force exists between the atoms of the tip and sample surfaces. The tip is pulled toward the sample and the contact occurs at point B. As the sample is pushed further against the tip, the force at the interface increases and the cantilever is deflected upward. This deflection equals the sample traveling

distance measured from point B for a rigid sample. As the sample is retracted, the force is reduced. At point D in the retracting curve, the sample is disengaged from the tip. Before the disengagement, the tip is pulled toward the downward direction due to the attractive force. The force required to pull the tip away from the sample is the force that equals (but in the opposite direction with) the adhesive force. This force is probably due to a layer of contaminant (such as water) on the sample surface (Mate et al., 1989; Blackman et al., 1990a). The horizontal shift between the loading and unloading curves results from the hysteresis of the PZT tube.

For a rigid sample, the cantilever deflection and the sample traveling distance (when the tip and sample come in contact) equal to each other. This corresponds a slope of 1 in the deflection curve toward the left side of contact point (point B). For a soft material, the slope could be less than 1, i.e., the cantilever deflection can be smaller than the sample traveling distance because the tip can indent into the sample. For a calendered magnetic tape, shortly after the sample touches the tip, the slope of this curve is less than 1 which suggests that the tape has been indented; as the load is increased, slope of the curve equals 1, Fig. 1a. This observation indicates that the surface of tape is soft locally (possibily polymer rich) but it is hard (as a result of uniform dispersion of magnetic particles) underneath. For an uncalendered magnetic tape, the cantilever deflection equals the sample traveling distance initially, but is smaller than the tape traveling distance as the load is increased. This suggests that tape surface is hard (particle rich) but it is soft underneath. Since the exact contact area is not known, the actual hardness value of the tapes can not be calculated. Typical behavior shown in Fig. 1a for the calendered tape was also observed at few locations in the uncalendered tape and the typical behavior shown in Fig. 1b for the uncalendered tape was also observed at few locations in the calendered tape. Both behaviors were observed in each of the two Co-γFe_2O_3 tapes.

As shown in Fig. 2, for both lubricated and unlubricated disks (as-polished), slope of the deflection curves is 1 and remains constant as the disks touch and continue to push the AFM tip.

Disks are not indented. The only difference between the two disks is that the pull-off force is larger for the lubricated disk than for the unlubricated disk. Pull-off force is determined by multiplying the cantilever spring constant (0.4 N/m) by the horizontal distance between points C and D, which corresponds to the maximum cantilever deflection towards the disks before the tip is disengaged. The horizontal distance/ pull-off force is larger for the lubricated disk (160 nm / 64 nN) than for unlubricated disk (105 nm /42 nN). This phenomenon was also observed for textured disks, where the pull-off forces were about 80 nN and 50 nN for the lubricated and unlubricated disks, respectively.

We observed topographic changes in the tapes at relatively high normal load (100 nN). Figure 3 shows the topography of a calendered metal-particle tape obtained at two different loads. For a given normal load, measurements were made twice. There was no discernible difference between consecutive measurements for a given normal load. However, as the load increased from 20 to 100 nN, material (indicated by an arrow) was pushed towards the right side in the sliding direction of the AFM tip relative to the sample. The material movement is believed to occur as a result of plastic deformation of the tape surface. Similar behavior was observed on all tapes. With disks, we did not notice any deformation under a 100 nN normal load.

Magnetic tape coating is made of magnetic particles and polymeric binder. Any movement of the coating material can eventually lead to loose debris. Debris formation is an undesirable situation as it may contaminate the head which may increase friction and/or wear between the head and tape, in addition to the deterioration of the tape itself.

3.2 Friction Measurements

Atomic-scale and macro friction data for all tapes and disks are presented in tables 1 and 2. We note that atomic-scale coefficient of friction of the uncalendered metal-particle tape is higher than that of a calendered tape, and wiped tape exhibits slightly higher atomic-scale friction than

unwiped tape, however, the opposite is true for macrofriction. Atomic-scale coefficient of friction of as-polished and textured disks are similar, however, macrocoefficient of friction of a textured disk is lower than that for as-polished disk. Lubricated disks exhibits lower atomic-scale and macrofriction than unlubricated disks. With a larger scan area, the atomic-scale coefficient of friction decreases in the case of tapes, but increases in the case of disks. We further note that in all cases, atomic-scale friction is smaller than the corresponding macrofriction.

Next, we examine the relationships between friction and roughness profiles. For selected data, see Figs. 4 to 7. For all tapes and disks measured, there is no resemblance between the coefficient of friction profiles and the corresponding roughness profiles, e.g., high or low points on the friction profile do not correspond to high or low points on the roughness profiles. However, spatial distribution of the two profiles appears to be similar, i.e., the top view of the two profiles appears to consist of "mosaics" of similar sizes. We calculated the slope of roughness profile in the tip sliding direction. The resulting *slope profiles*, along with the corresponding roughness and friction profiles are plotted in Figs. 4, 6, and 7 ,which correspond to data for a calendered metal-particle tape, a textured and an as-polished lubricated disks, respectively. By comparisons of the slope and friction profiles, we observe a strong correlation between the two. Also see Figs. 10 and 11, to be presented later. As shown in Fig. 5, this correlation is also seen from the similar power spectrum density functions of the slope and friction profiles. The relative intensity of high frequency components of the friction profiles is larger than that of the corresponding roughness profile. This is consistent with the discussion that friction variation resembles the variation of the slope (derivative) of surface roughness. In general, the relative amplitude of each frequency component is magnified by a factor proportional to the frequency going from a function to its derivative function.

To further verify the relationship between surface slope and microfriction values, and to eliminate any effect resulting from nonuniform composition of tape and disk surfaces, we

measured a polished natural (IIa) diamond. Repeated measurements were made along one line on the surface. Highly reproducible data were obtained. We present roughness profile, the slope of the roughness profile, and the friction profile of diamond in Fig. 8. Again the variation of friction does correlate to the variation of the slope of the roughness profile taken along the sliding direction of the tip.

We now examine the mechanism of atomic-scale friction which may explain the resemblance between the slope of surface roughness profiles and the corresponding friction profiles. There are three dominant mechanisms of friction: adhesive, adhesive and roughness (ratchet), and ploughing. As a first order, we may assume these to be additive. Adhesive mechanism alone cannot explain the local variation in friction. Let us consider the ratchet mechanism. According to Bowden and Tabor (1950) and Tabor (1979), we consider a small tip sliding over an asperity making an angle θ with the horizontal plane, Fig. 9. The normal force (normal to the general surface) applied by the tip to the sample surface W is constant. Friction force F on the sample varies as a function of the surface roughness. It would be a constant $\mu_0 W$ for a smooth surface in the presence of "adhesive" friction mechanism. The force components along (S) and perpendicular to (N) the local surface of the sample at the contact point are,

$$N = W\cos\theta + F\sin\theta \qquad (1)$$

$$S = F\cos\theta - W\sin\theta. \qquad (2)$$

Since, when sliding occurs, $S/N = \mu_0$ (adhesive coefficient of friction without roughness effect), we obtain the value of coefficient of friction because of adhesive and roughness (ratchet) effects

$$\mu_1 = F/W = (\mu_0 + \tan\theta)(1-\mu_0 \tan\theta), \qquad (3a)$$

where μ_1 is the local coefficient of friction. Since μ_0 is small on an atomic scale, Eq. (3a) can be rewritten as

$$\mu_1 \sim \mu_0 + \tan\theta, \qquad (3b)$$

indicating that in ascending the slope one may simply add the adhesion and the asperity term to one another. Similarly, on the right hand side (descending part) of the asperity,

$$\mu_2 = (\mu_0 - \tan\theta)(1+\mu_0 \tan\theta) \quad (4a)$$

$$\sim \mu_0 - \tan\theta, \quad (4b)$$

if μ_0 is small. For a symmetrical asperity, the average coefficient of friction the AFM tip experienced in traveling across the whole asperity is

$$\mu_{ave} = (\mu_1+\mu_2)/2$$

$$=\mu_0(1+\tan^2\theta)/(1-\mu_0^2\tan^2\theta) \quad (5a)$$

$$\sim\mu_0(1+\tan^2\theta), \quad (5b)$$

if μ_0 is small. The ploughing component of friction (Bowden and Tabor 1950) with tip sliding in either direction,

$$\mu_p\sim\tan\theta. \quad (6)$$

Since in the FFM measurements, we notice little damage of the sample surface, the contribution by ploughing is expected to be negligible and the ratchet mechanism is believed to be the dominant mechanism for the local variations in the friction profile. With the tip sliding over the leading (ascending) edge of an asperity, the slope is positive, it is negative during sliding over the trailing (descending) edge of the asperity. Thus, friction is high at the leading edge of asperities and low at the trailing edge. The ratchet mechanism thus explain the correlation between slopes of the roughness profiles and friction profiles observed in Figs. 4, 6 to 8. We note that in the ratchet mechanism, AFM tip is assumed to be small as compared to the size of asperities. This is valid since the typical radius of curvature of the tips is about 30 nm. The radius of curvature of the asperities of the samples measured here (the asperities that produce most of the friction variation) is found to be typically about 100-200 nm which is larger than that of the AFM tip (Bhushan and Blackman, 1991). Lower values of atomic-scale friction as compared to macrofriction may be because of less ploughing contribution in microfriction measurements.

Since the local coefficient of friction μ is a function of the local slope of sample surface, the local μ can thus be different as the scanning direction of the sample is reversed. Figures 10 and 11 show the gray scale plots of slope of roughness profiles and friction profile for a calendered metal-

particle tape and an unlubricated textured disk, respectively. The left side of the figures corresponds to the sample sliding from the right towards the left. The right side of the figures corresponds to the sample sliding from left towards the right (the slopes were taken opposite to the sample sliding directions). We note that generally the points which have high friction in the left to right scan have low friction as the sliding direction is reversed. This relationship is not true at some locations. Thus, directionality in local variation of the atomic friction data is observed.

If asperities in a sample surface have a preferential orientation, this directionality effect will be manifested in macroscopic friction data, that is, the coefficient of friction may be larger in one sliding direction than that in the other direction. Such phenomenon has been observed in rubbing wool fiber against horn. It was found that the coefficient of friction is greater when the wool fiber is rubbed towards its root than when it is rubbed towards its tip (Mercer,1945; Lipson and Mercer, 1946; Thomson and Speakman, 1946; Bowden and Tabor 1950). Makinson (1947) explained the directionality in the friction by the *"ratchet" effect. Here,* the ratchet effect is the result of large angle θ, where instead of true sliding, rupture or deformation of the fine scales of wool fiber occurs in one sliding direction. We note that the frictional directionality can also exist in materials with particles having a preferred orientation.

4. Summary

We have conducted nanoindentation, nanoscratch, and atomic-scale friction studies on magnetic tapes and disks using AFM/FFM. The hardness of the tapes was found to be nonuniform through the coatings. Localized plastic deformation of tapes was observed under about 100 nN applied normal load. We found a strong correlation between slope of the surface profile (in the sliding direction) and the atomic-scale friction profile. We also observed directionality in the local variation of atomic-scale friction and noted that atomic-scale friction values are generally lower than that of the corresponding macro friction values.

Acknowledgments

We thank Dr. V. Koinkar for some of the atomic-scale friction measurements, and to Dr. B. K. Gupta and Mr. S. Patton for macrofriction measurements. This project was sponsored by the Department of the Navy, Office of the Chief of Naval Research. The contents of the information does not necessarily reflect the position or the policy of the Government, and no official endorsement should be inferred.

References

Andoh, Y., Oguchi, S., Kaneko, R. and Miyamoto, T. (1992), "Evaluation of Very Thin Lubricant Films", J. Phys. D: Appl. Phys. Vol. 25, pp. A71-A75

Bhushan, B. (1990), Tribology and Mechanics of Magnetic Storage Devices, Springer-Verleg, New York.

Bhushan, B. and Blackman, G. S. (1991), "Atomic Force Microscopy of Magnetic Rigid Disks and Sliders and Its Application to Tribology" J. Trib., Trans. ASME, Vol. 113, pp. 452-457.

Bhushan, B., Dominiak, M. and Lazzari, J. P., (1992), "Contact-Start-Stop Studies with Silicon Planner Head Sliders Against Thin Film Disks", IEEE Trans. Magn., Vol. 28, pp. 2874-2876.

Bhushan, B. and Venkatesan, S. (1993), "Friction and Wear Studies of Silicon in Sliding Contact with Thin-Film Magnetic Disks", J. Mat. Res. (in press).

Blackman, G. S., Mate, C. M. and Philpott (1990a), "Interaction Force of a Sharp Tungsten Tip with Molecular Films on Silicon Surfaces" Phys. Rev. Lett. Vol. 65, No. 18, pp. 2270-2273.

Blackman, G. S., Mate, C. M. and Philpott, M. R. (1990b), "Atomic Force Microscope Studies of Lubricant Films on Solid Surfaces", Surface Sci. Vol. 41, pp. 1283-1286.

Bowden, F. P. and Tabor, D. (1950), The Friction and Lubrication of Solids, Clarendon Press, Oxford, pp. 172-175.

Hamada, E. and Kaneko, R. (1992), "Microdistortion of Polymer Surfaces by Friction", J. Phys. D.: Appl. Phys. Vol. 25, pp. A53-A56.

Kaneko, R. (1988), "A Frictional Microscope Controlled with an Electromagnet", J. Microscopy, Vol. 152, Pt. 2, pp. 363-369.

Kaneko, R., Miyamoto, T. and Hamada, E. (1991), "Development of a Controlled Friction Force Microscope and Imaging of Recording Disk Surfaces", Adv. Inf. Storage Syst., Vol. 1, pp. 267-277.

Lipson, M. and Mercer, E. H. (1946), "Frictional Properties of Wool Treated with Mercuric Acetate", Nature, Vol. 157, pp. 134-135.

Mate, C. M. (1992), "Nanotribology Studies of Carbon Surfaces by Force Microscopy", Proc. 1st International Workshop on Microtribology, The Jap. Soc. of Tribologists, Japan, pp. 230-238.

Mate, C. M., McClelland, G. M., Erlandsson, R., and Chiang, S. (1987), "Atomic-Scale Friction of a Tungsten Tip on a Graphite Surface", Phys. Rev. Lett. Vol. 59, No. 17, pp.1942-1945.

Mate, C. M., Lorenz, M. R. and Novotny, V. J. (1989), "Atomic Force Microscopy of Polymeric Liquid Films", J. Chem. Phys. Vol. 90, No. 12, pp. 7550-7555.

Makinson, K. R. (1948), "On the Cause of the Frictional Difference of the Wool Fiber", Trans. Faraday Soc. Vol. 44, pp. 279-282.

Mercer, E. H. (1945), "Frictional Properties of Wool Fibers", Nature, Vol. 155, pp. 573-574.

Meyer, G. and Amer, N. M. (1988), "Novel Optical Approach to Atomic Force Microscopy", Appl. Phys. Lett., Vol. 53, No. 12, pp. 1045-1047.

Meyer, G. and Amer, N. M. (1990), Simultaneous Measurement of Lateral and Normal Forces with an Optical-Beam-Deflection Atomic Force Microscope", Appl. Phys. Lett., Vol. 57, No. 20, pp. 2089-2091.

Miyamoto, T., Kaneko, R. and Ando, Y. (1990), "Interaction Force Between Thin Film Disk Media and Elastic Solids Investigated by Atomic Force Microscope" J. Trib., Trans. ASME, Vol. 112, pp. 567-572.

Oden, P. I., Majumdar, A., Bhushan, B., Padmanabhan, A. and Graham, J. J. (1992), "AFM Imaging, Roughness Analysis and Contact Mechanics of Magnetic Tape and Head Surfaces", J. Trib., ASME, Vol. 114, pp. 666-674.

Ruan, J. and Bhushan, B. (1993), "Atomic-Scale Friction Measurements Using Friction Force Microscopy, Part I - General Principles and New Measurement Techniques", Submitted to J. Trib. for publication.

Tabor, D. (1979), "Adhesion and Friction" in The Properties of Diamond (Field, J. E., editor), Academic, New York, pp. 325-350.

Thomson, H. M. S., and Speakman, J. B. (1946), "Frictional Properties of Wool", Nature, Vol. 157, p. 804.

Figure Captions

Fig. 1 Indentation curves of two metal-particle tapes (a) calendered, (b) uncalendered.

Fig. 2 Indentation curves of (a) unlubricated and (b) lubricated textured disks. The pull-off force is larger in the lubricated disk (64 nN) than in the unlubricated disk (42 nN) calculated from the horizontal distance between points C and D and the cantilever spring constant of 0.4 N/m.

Fig. 3 Surface roughness profiles of a calendered metal-particle magnetic tape. The applied normal force was 10 nN and 100 nN for (a) and (b) respectively. Location of the change in surface topography as a result of microscratch is indicated by arrows.

Fig. 4 (a) Surface roughness profile (σ= 7.9 nm), (b) slope of the roughness profile taken along the sample sliding direction (the horizontal axis) (mean= -0.006, σ= 0.300), and (c) friction profile (mean= 5.5 nN, σ= 2.2 nN) of a calendered metal-particle tape for a normal load of 70 nN. There is poor correlation between the surface roughness and friction. However, the slope of the roughness profile has an excellent correlation with the friction profile. (σ is the standard deviation).

Fig. 5 Frequency spectrum of (a) the surface roughness, (b) slope of the roughness, and (c) friction profile shown in Fig. 4. Vertical scale is logarithmic.

Fig. 6 (a) Surface roughness profile (σ= 4.4 nm), (b) slope of the roughness profile taken along the sample sliding direction (mean= 0.023, σ= 0.197), and (c) friction profile of a textured and lubricated disk (mean= 6.2 nN, σ= 2.1 nN) for a normal load of 160 nN.

Fig. 7 (a) Surface roughness profile (σ= 1.9 nm), (b) slope of the roughness profile taken along the sample sliding direction (mean= 0.001, σ= 0.111), and (c) friction profile of an as-polished and lubricated disk (mean=6.0 nN, σ= 1.5 nN) for a normal load of 160 nN.

Fig. 8 Surface roughness profile (σ=15.4 nm), slope of the roughness profile (mean=-0.052, σ=0.224) and friction profile (σ=2.1 nN) of a polished natural (IIa) diamond crystal. The slope of the roughness profile closely resembles the friction profile.

Fig. 9 Schematic illustration showing the effect of an asperity (making an angle θ with the horizontal plane) on the surface in contact with the tip on local friction in the presence of "adhesive" friction mechanism (Tabor, 1979).

Fig. 10 Gray-scale plots of (a) the slope of the surface roughness and (b) the friction of a calendered metal-particle tape. The left side of the figure corresponds to the sample sliding from right to left and the right side of the figure corresponds the sample sliding from left to right. Higher points (in friction or in roughness slope) are shown by lighter color.

Fig. 11 Gray-scale plots of (a) the slope of the surface roughness and (b) the friction of a lubricated textured disk. The left side of the figure corresponds to the sample sliding from right to left and the right side of the figure corresponds the sample sliding from left to right. Higher points are shown by lighter color.

Table 1. Surface roughness and atomic-scale and macro friction data of magnetic tape samples

Samples		RMS (nm)			Atomic-scale coefficient of friction		Macro Coefficient of friction against:	
		NOP	AFM					
		250 μm	1 μm	10 μm	1 μm	10 μm	Ni-Zn Ferrite	Si_3N_4
Metal-particle tapes	calendered	6.0	6.1	11.7	0.08	0.07	0.29	0.22
	uncalendered	12.0	13.5	25.6	0.11	0.10	0.23	0.14
Co-γFe_2O_3 tapes	unwiped	11.0	8.0	12.9	0.06	0.04	0.43	0.32
	wiped	15.4	10.2	15.0	0.07	0.06	0.35	0.22

Table 2 Surface roughness and atomic-scale and macro friciton data of magnetic disk samples

Disk I.D.	RMS (nm)			Atomic-scale coefficient of friction		Macro coefficient of friciton
	NOP	AFM				
	250 μm	1 μm	10 μm	1 μm	10 μm	against Al_2O_3-TiC
Unlubricated disk (as-polished)	2.2	3.3	4.5	0.05	0.06	0.26
Unlubricated disk (standard texture)	4.2	4.4	9.3	0.05	0.06	0.24
Lubricated disk (as-polished)	2.3	2.3	4.1	0.04	0.05	0.19
Lubricated disk (standard texture)	4.6	5.4	8.7	0.04	0.05	0.16

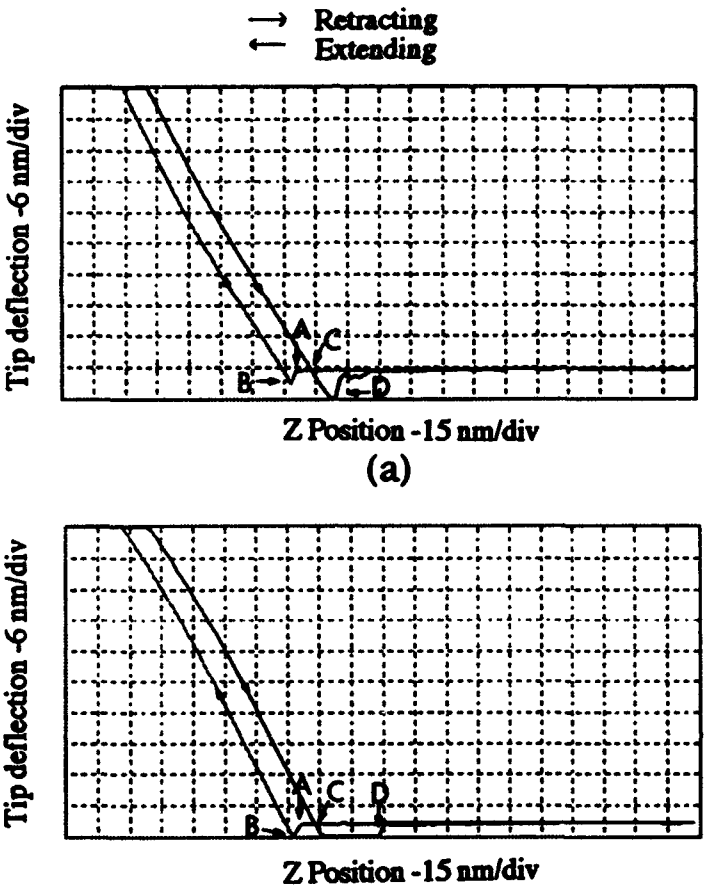
→ Retracting
← Extending
Tip deflection -6 nm/div
A
C
B
D
Z Position -15 nm/div
(a)
Tip deflection -6 nm/div
A
C
D
B
Z Position -15 nm/div
(b)

Fig. 1

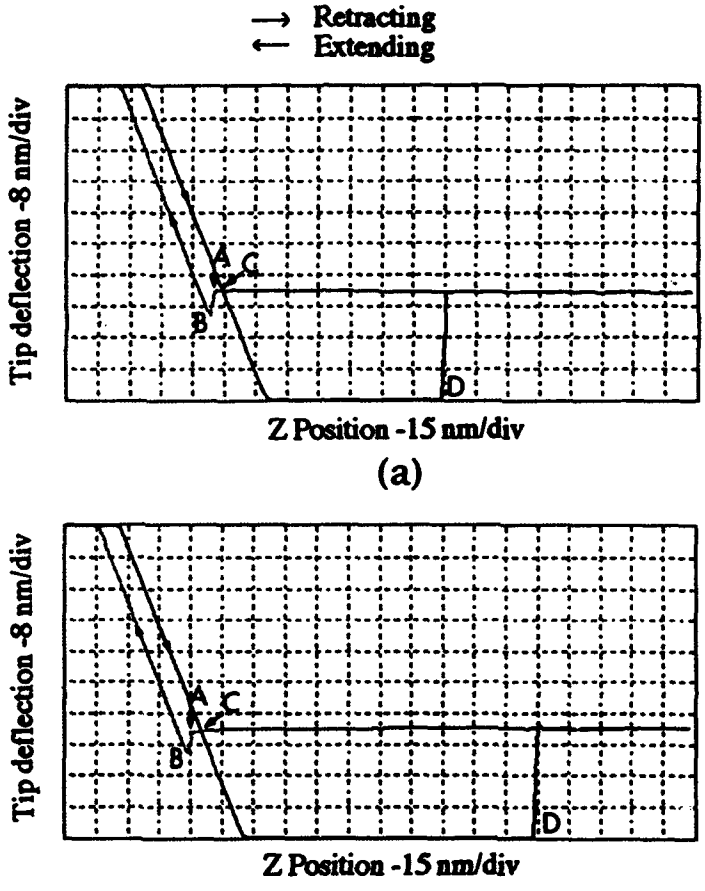
→ Retracting
← Extending
Tip deflection -8 nm/div
A
C
B
D
Z Position -15 nm/div
(a)
Tip deflection -8 nm/div
A
C
B
D
Z Position -15 nm/div
(b)

Fig. 2

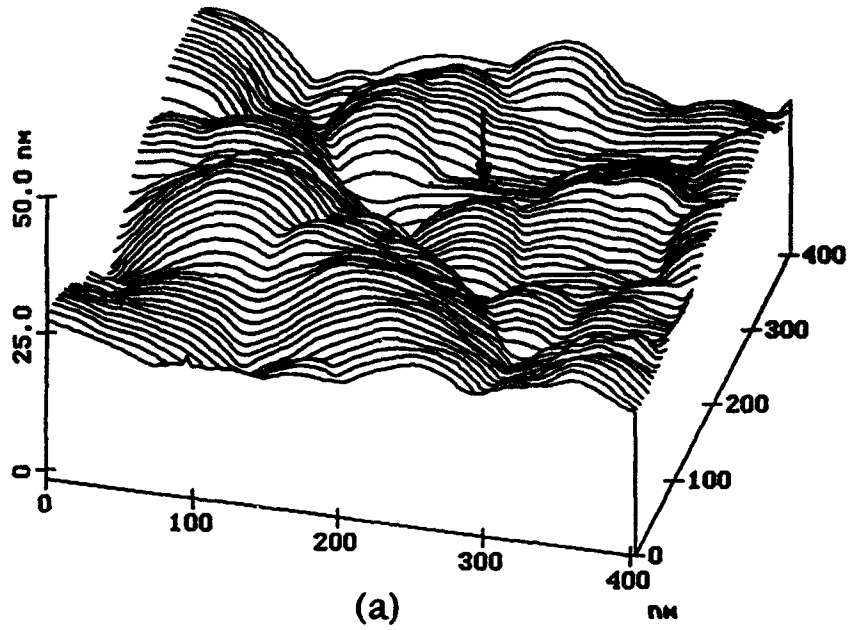
50.0 nm
25.0
0
0
100
200
300
400
0
100
200
300
400
nm

(a)

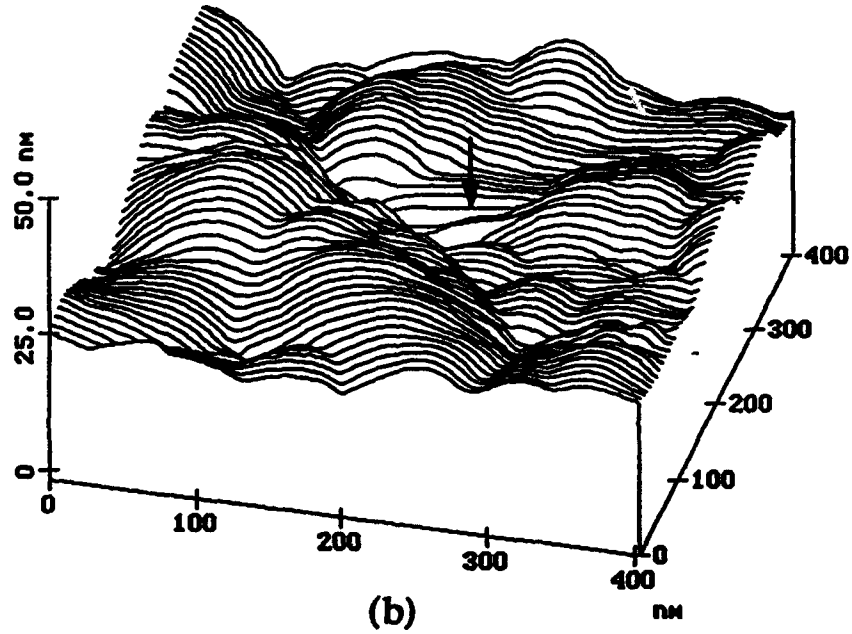
50.0 nm
25.0
0
0
100
200
300
400
0
100
200
300
400
nm

(b)

Fig. 3

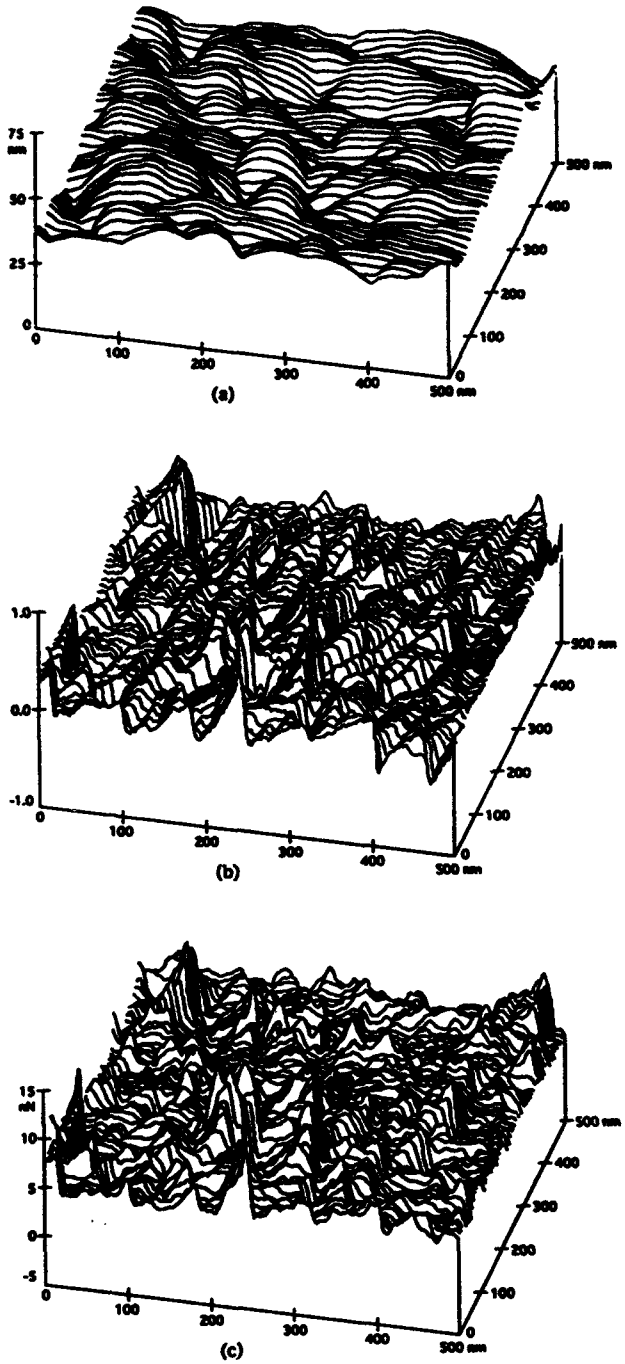
75
nm
50
25
0
0
100
200
300
400
500 nm
0
100
200
300
400
500 nm
(a)
1.0
0.0
-1.0
0
100
200
300
400
500 nm
0
100
200
300
400
500 nm
(b)
15
nM
10
5
0
-5
0
100
200
300
400
500 nm
0
100
200
300
400
500 nm
(c)

Fig. 4

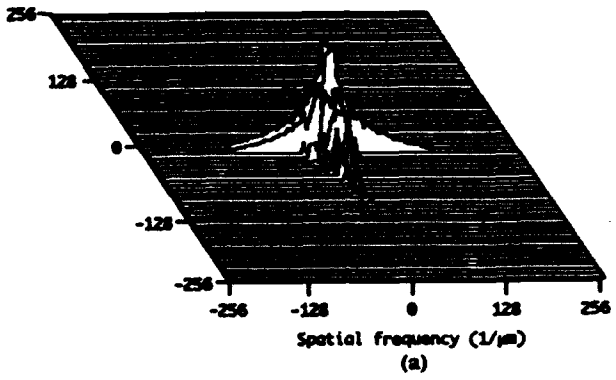
256
128
0
-128
-256
-256
-128
0
128
256
Spatial frequency (1/μm)
(a)

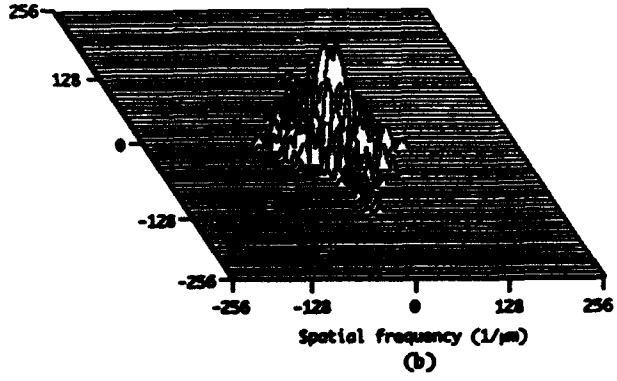
256
128
0
-128
-256
-256
-128
0
128
256
Spatial frequency (1/μm)
(b)

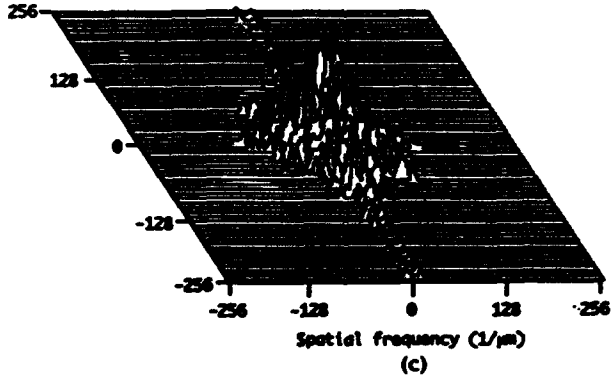
256
128
0
-128
-256
-256
-128
0
128
256
Spatial frequency (1/μm)
(c)

Fig. 5

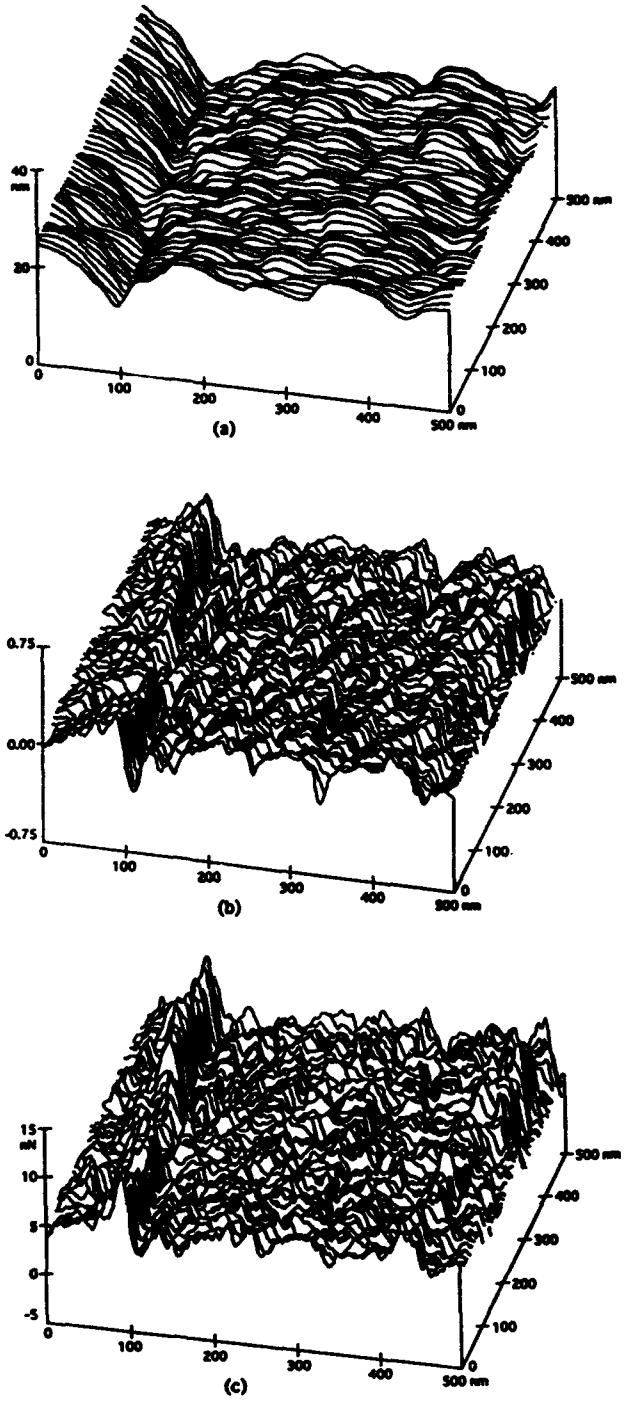
40
nm
20
0
0
100
200
300
400
500 nm
500 nm
400
300
200
100
0
(a)
0.75
0.00
-0.75
0
100
200
300
400
500 nm
500 nm
400
300
200
100
0
(b)
15
nM
10
5
0
-5
0
100
200
300
400
500 nm
500 nm
400
300
200
100
0
(c)

Fig. 6

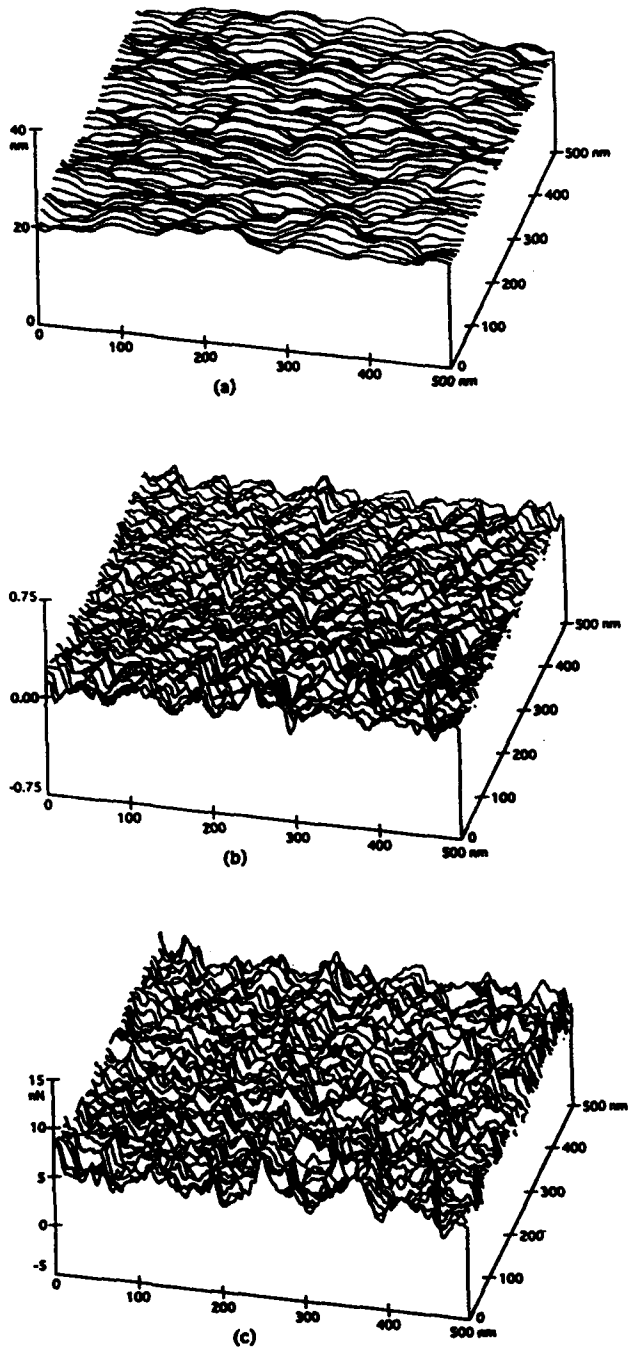
40
nm
20
0
0
100
200
300
400
500 nm
500 nm
400
300
200
100
0
(a)
0.75
0.00
-0.75
0
100
200
300
400
500 nm
500 nm
400
300
200
100
0
(b)
15
nM
10
5
0
-5
0
100
200
300
400
500 nm
500 nm
400
300
200
100
0
(c)

Fig. 7

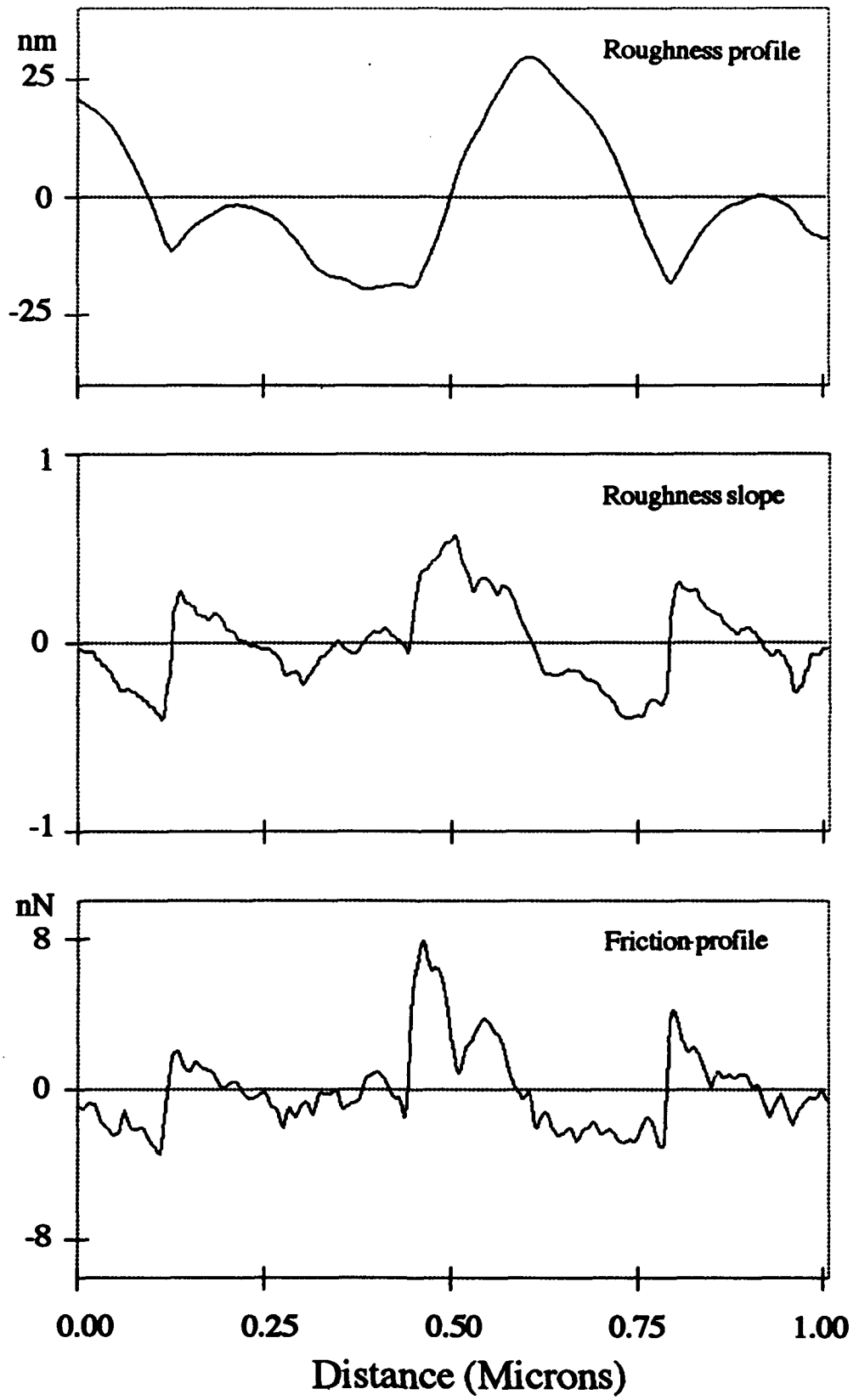
nm
25
0
-25
Roughness profile
1
0
-1
Roughness slope
nN
8
0
-8
Friction profile
0.00
0.25
0.50
0.75
1.00
Distance (Microns)

Fig. 8

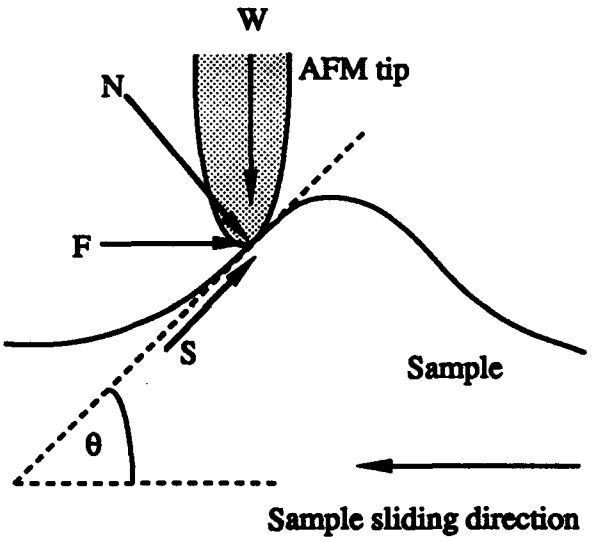

Fig. 9

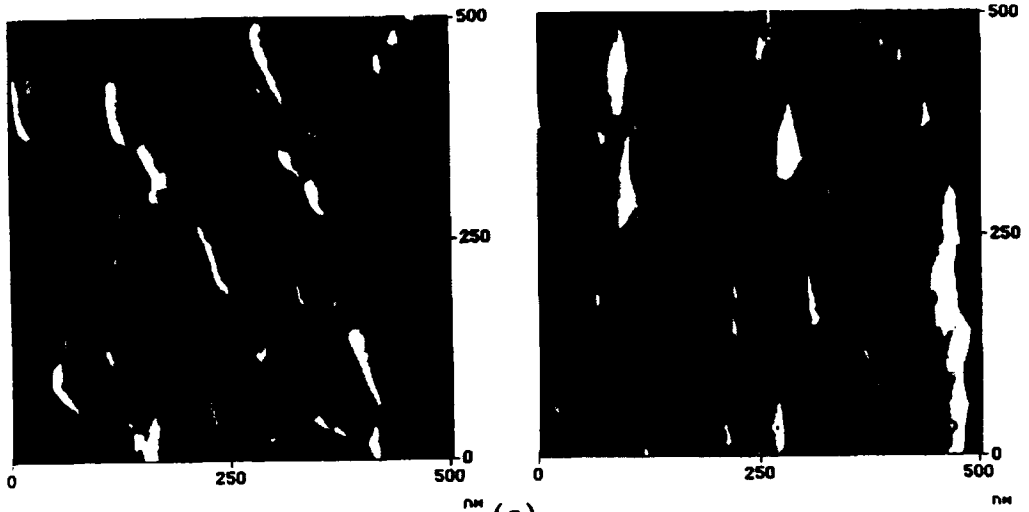

(a)

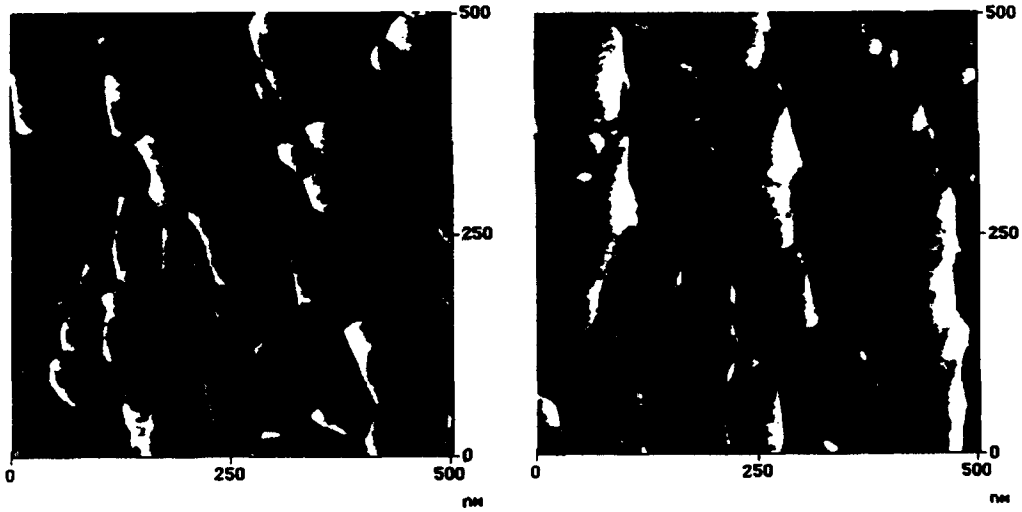

(b)

Fig. 10

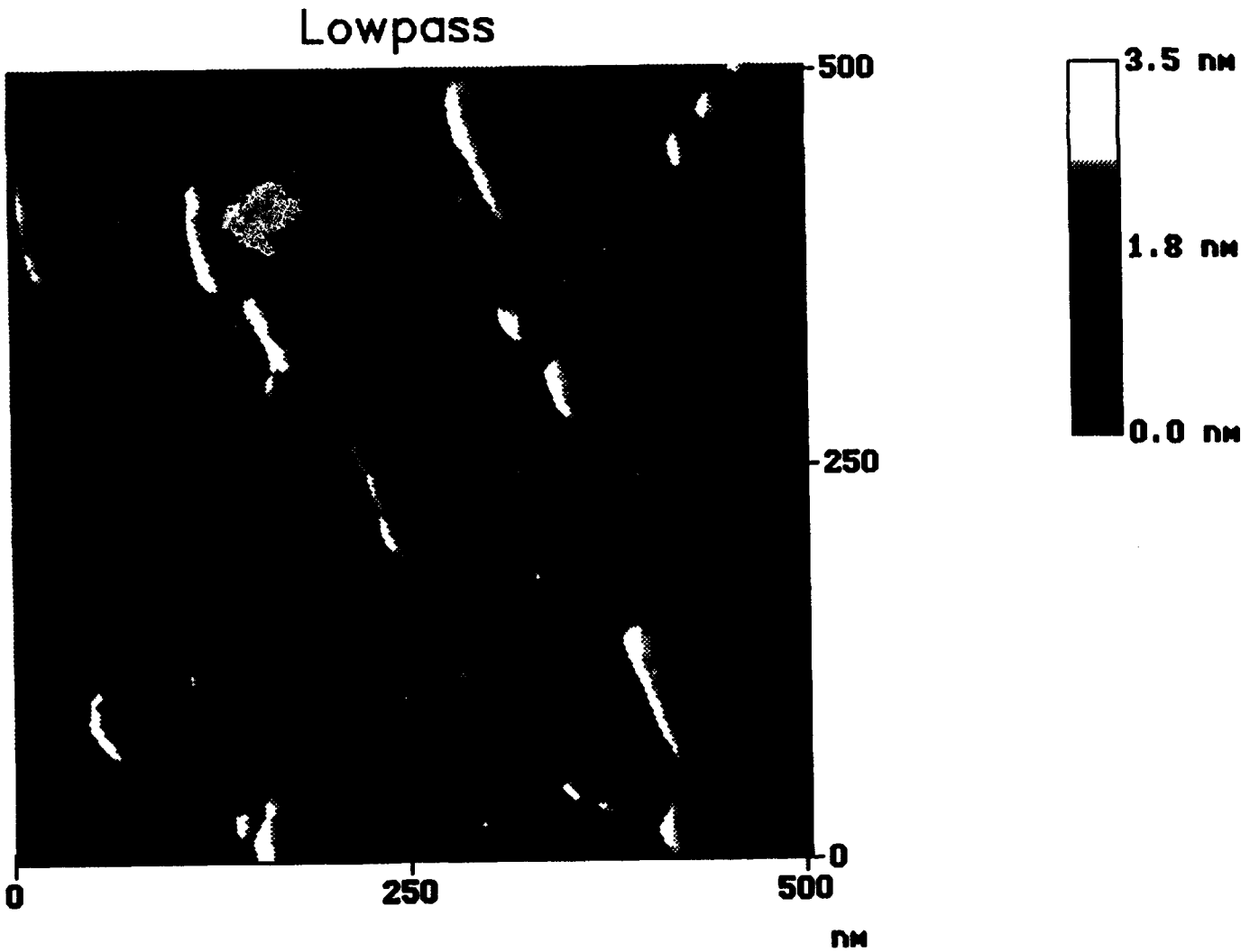

Fuji Calendered tape, trace

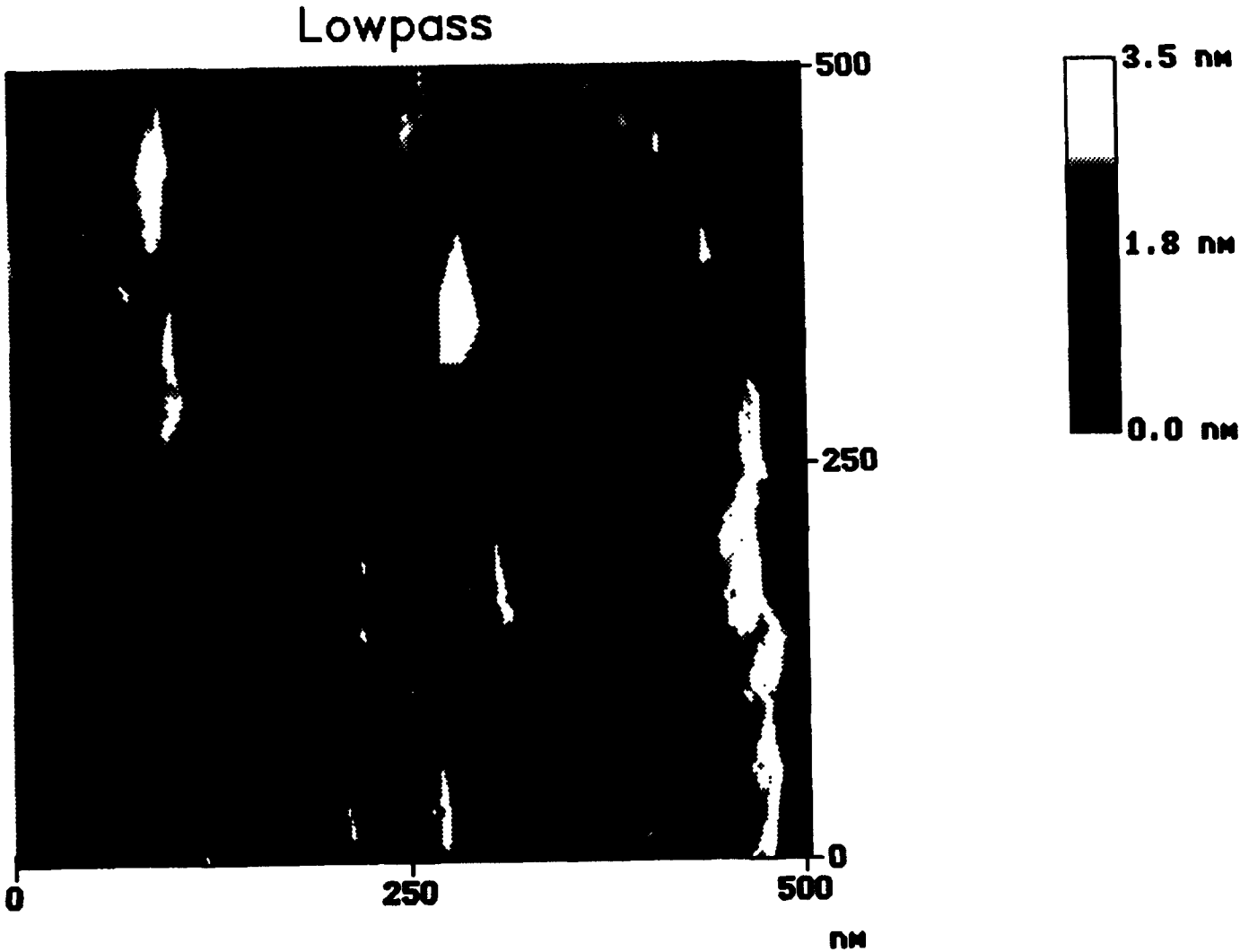

Fuji M.P. tape, calendered. Retrace

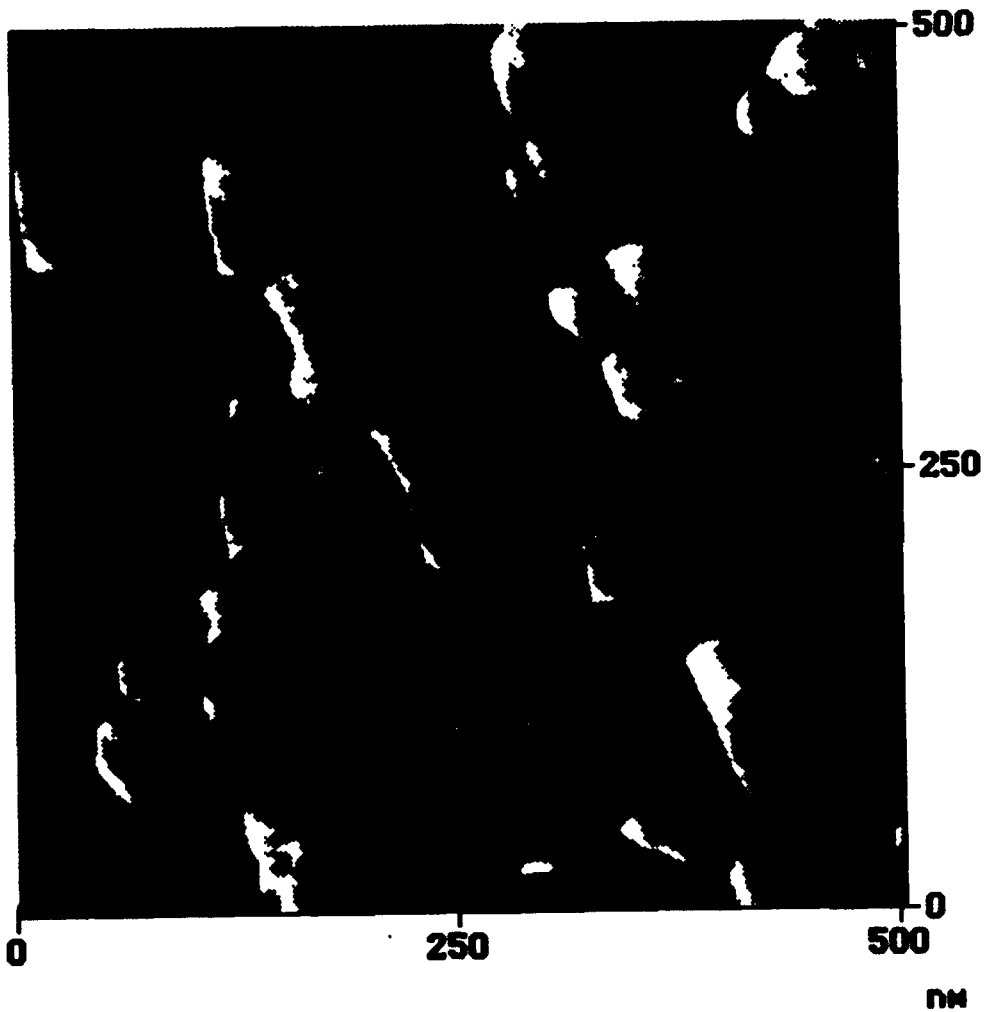

Fuji Calendered tape, trace

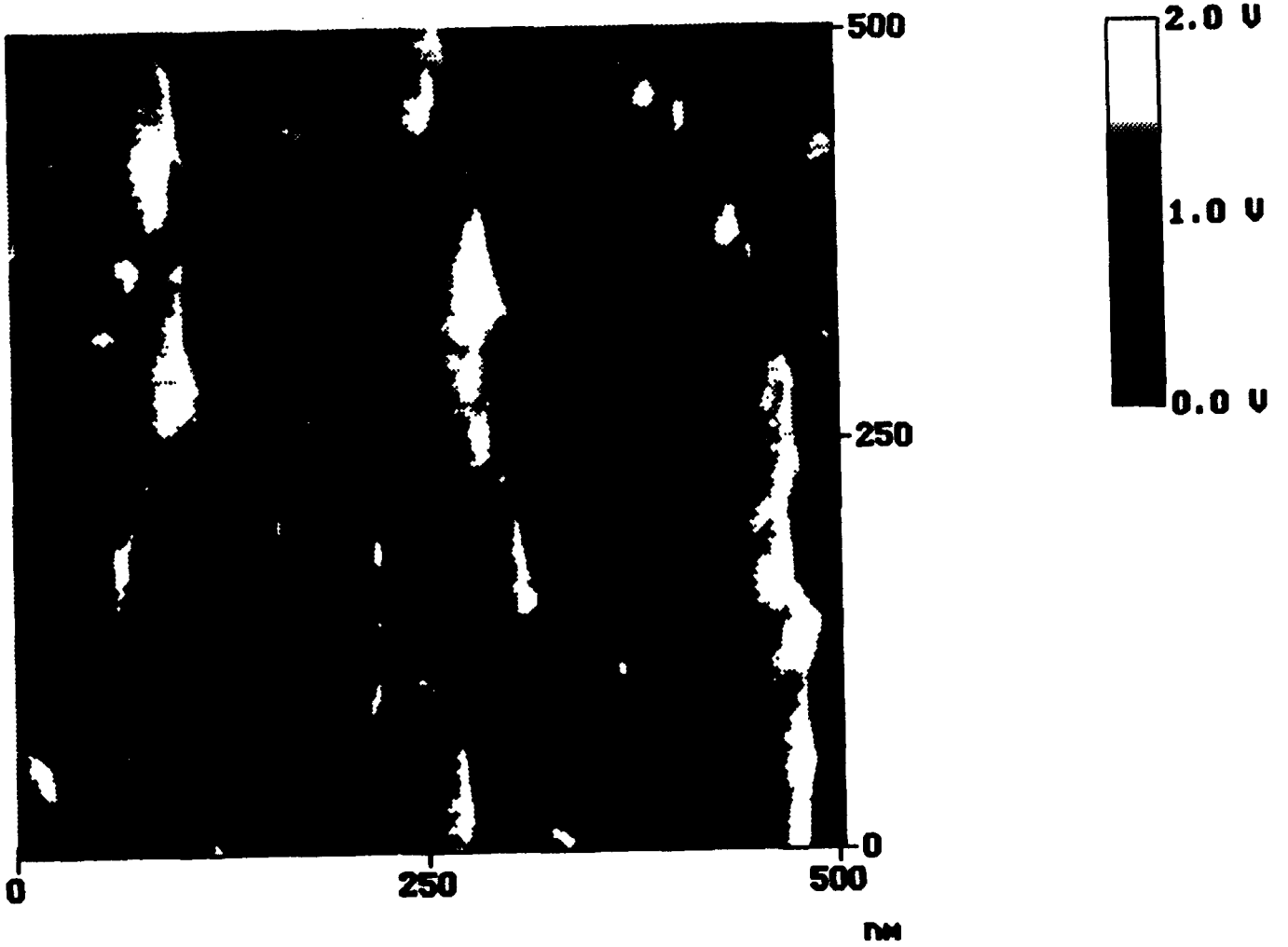

Fuji M.P. tape, calendered. Retrace

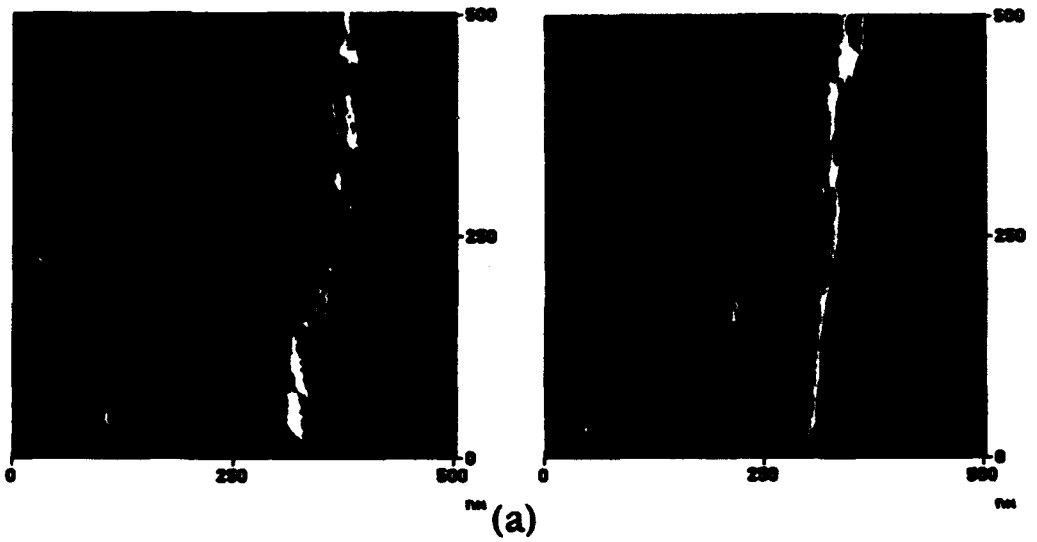

(a)

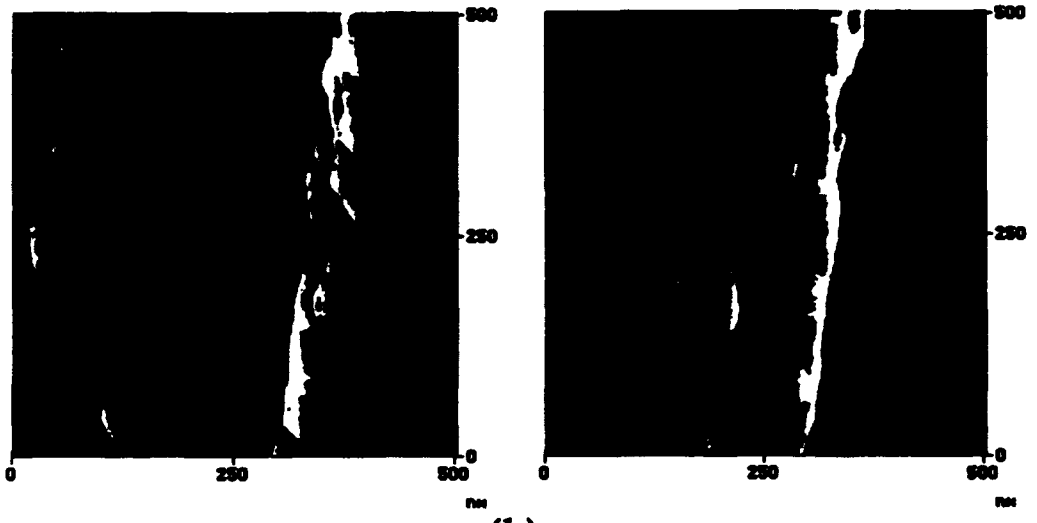

(b)

Fig. 11

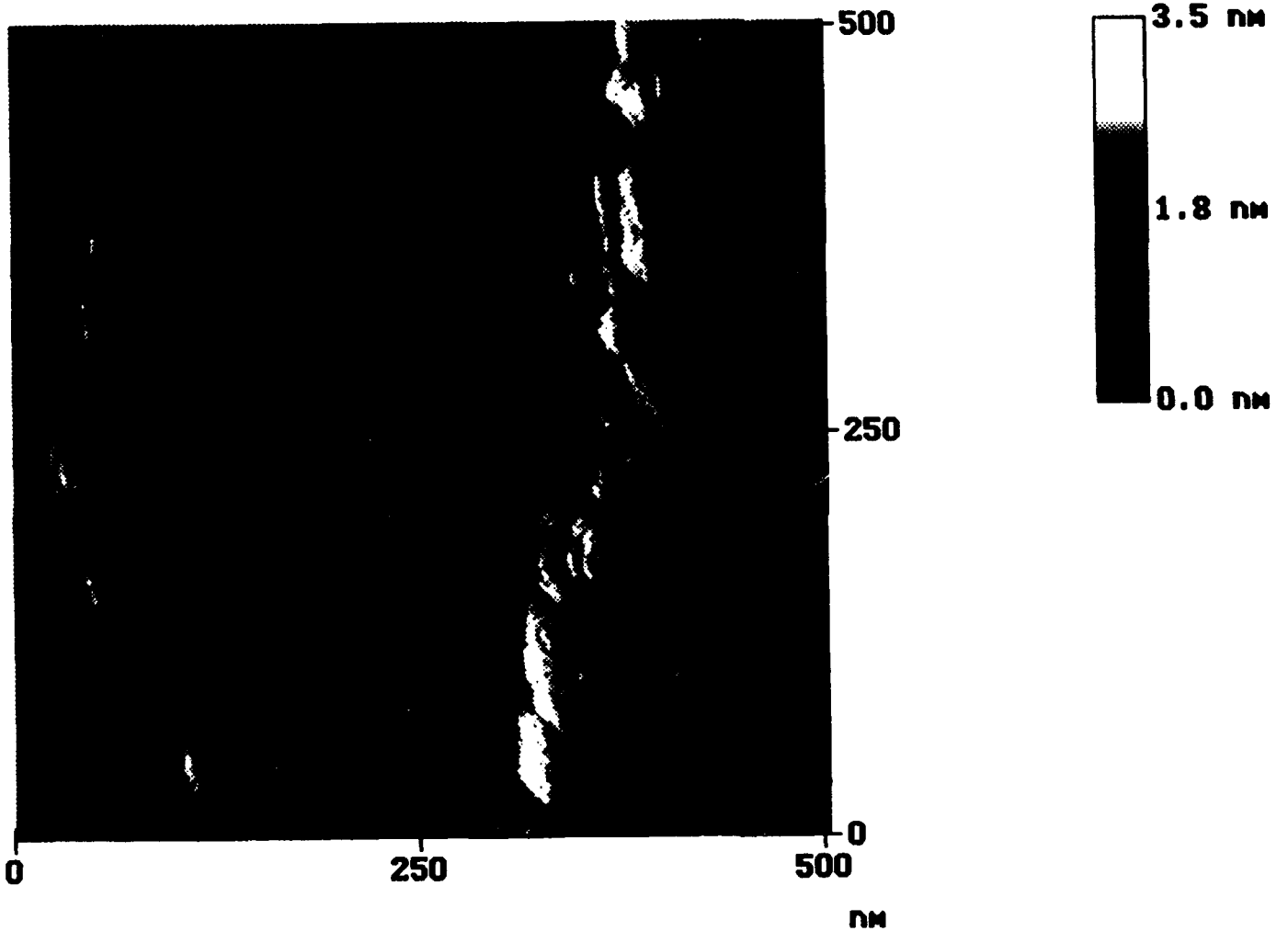

Lubricated textured disk, Trace

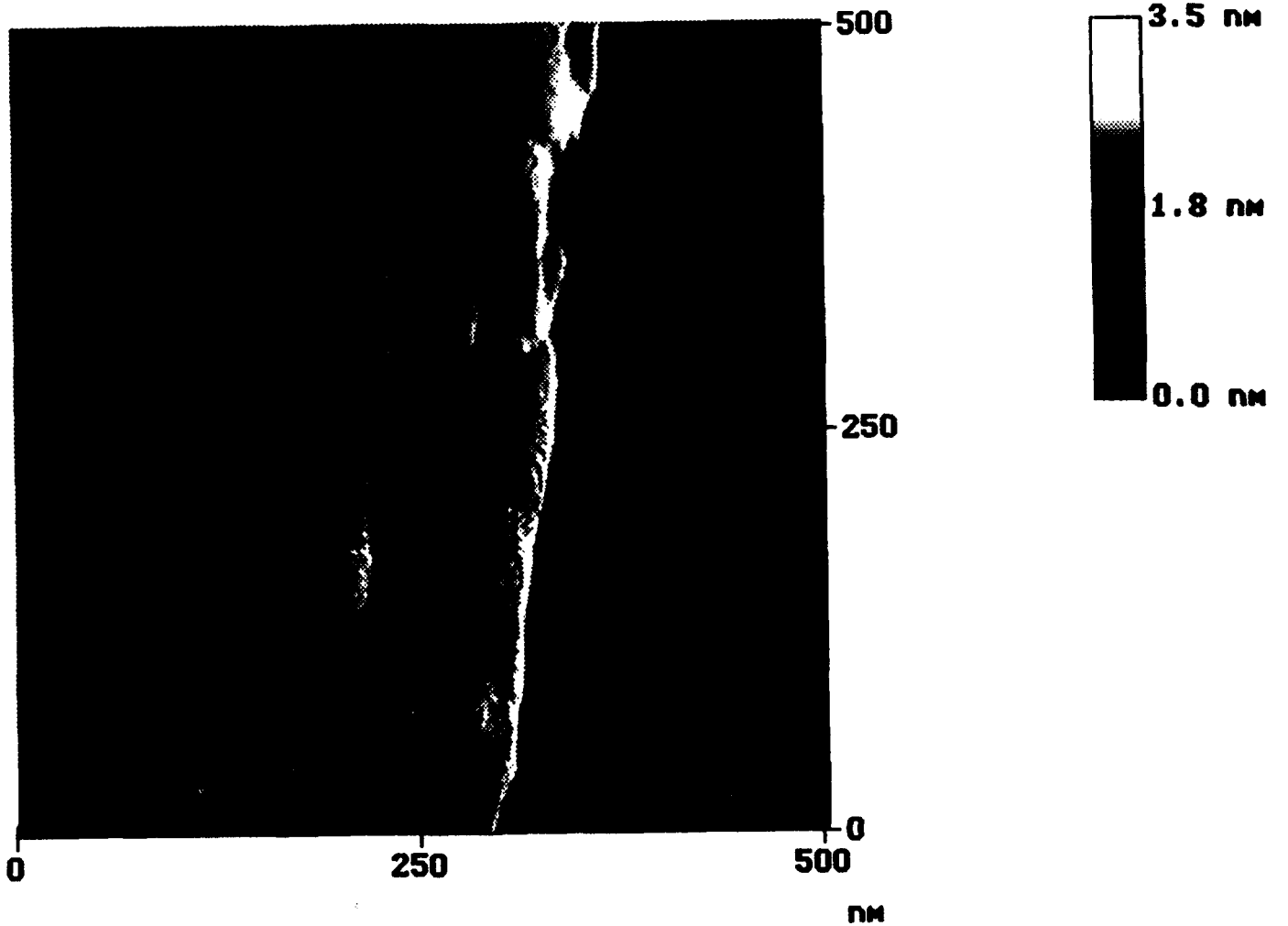

Lubricated textured disk, Retrace

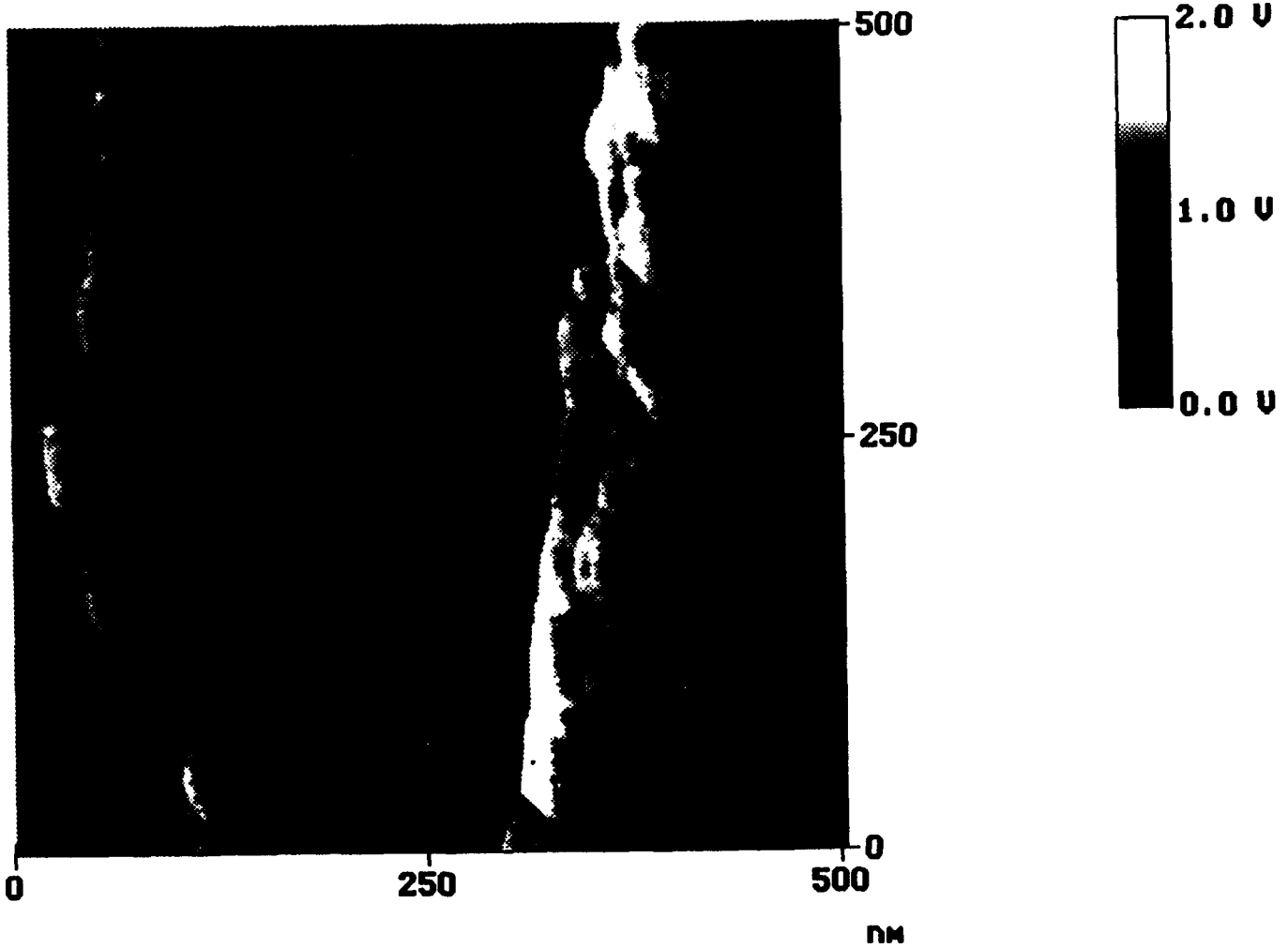

Lubricated textured disk, Trace

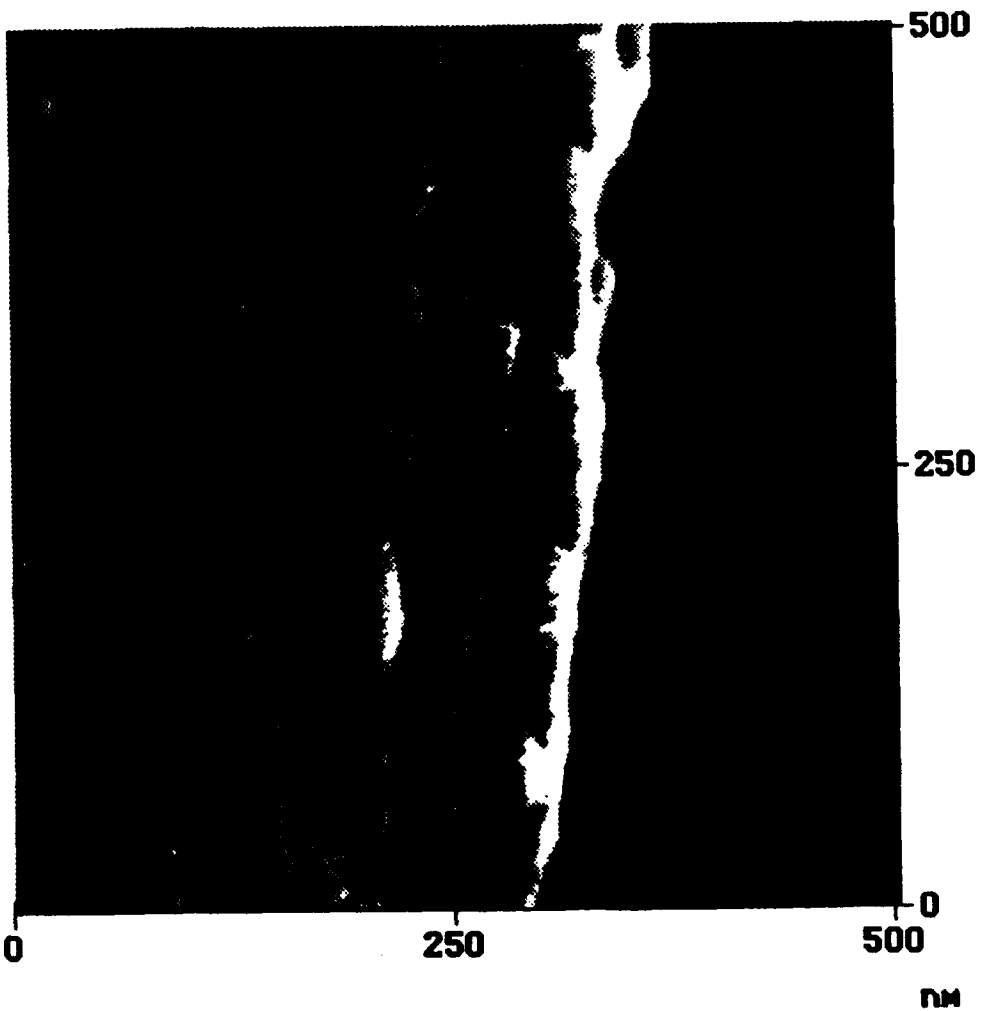

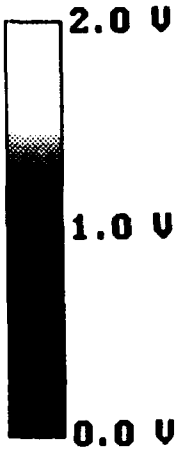

Lubricated textured disk, Retrace